

See discussions, stats, and author profiles for this publication at: <https://www.researchgate.net/publication/255772296>

# Effects of molecular structures and solvent properties on the self-assembly of carbazole-based conjugated dendrimers by solvent vapor annealing

ARTICLE *in* RSC ADVANCES · MAY 2013

Impact Factor: 3.84 · DOI: 10.1039/C3RA23272G

---

CITATIONS

5

---

READS

19

## 8 AUTHORS, INCLUDING:



Zicheng Ding

Chinese Academy of Sciences

17 PUBLICATIONS 94 CITATIONS

[SEE PROFILE](#)



Rubo Xing

Chinese Academy of Sciences

57 PUBLICATIONS 883 CITATIONS

[SEE PROFILE](#)



Xingdong Wang

Chinese Academy of Sciences

13 PUBLICATIONS 103 CITATIONS

[SEE PROFILE](#)



Lixiang Wang

Chinese Academy of Sciences

292 PUBLICATIONS 7,311 CITATIONS

[SEE PROFILE](#)

Cite this: *RSC Advances*, 2013, 3, 8037

## Effects of molecular structures and solvent properties on the self-assembly of carbazole-based conjugated dendrimers by solvent vapor annealing<sup>†</sup>

Zicheng Ding,<sup>a</sup> Rubo Xing,<sup>a</sup> Yue Sun,<sup>a</sup> Lidong Zheng,<sup>a</sup> Xingdong Wang,<sup>a</sup> Junqiao Ding,<sup>a</sup> Lixiang Wang<sup>a</sup> and Yanchun Han<sup>\*ab</sup>

The effects of molecular structures and solvent properties on the self-assembly behavior of carbazole-based conjugated dendrimers by solvent vapor annealing (SVA) were systematically studied. Different film morphology changes from three different carbazole dendrimers through annealing in tetrahydrofuran (THF) and hexane vapor, two solvents with approximately the same vapor pressure but different polarity, were observed. For the first generation dendrimer H1-BCz, the film morphology was changed from random single fibers to spherulites with a decrease of vapor pressure in THF vapor, while only curled fibers and dendrites formed in hexane vapor. For the second generation dendrimer H2-BCz, the film morphology was not changed at low vapor pressure conditions, only fibers formed in THF vapor and nano-sized needle-like aggregates formed at high vapor pressure in hexane vapor. For the second generation dendrimer H28 with *n*-octyl instead of *tert*-butyl as the surface groups, only dewetting took place. Through a comparative study of the morphologies and the spectra of the annealed films, we speculated that the molecule–solvent and molecule interactions dominate for H1-BCz films, the molecule–molecule interaction is predominant for H2-BCz films and the solvent–molecule interaction controls the dewetting process of H28 films.

Received 11th December 2012,  
Accepted 18th March 2013

DOI: 10.1039/c3ra23272g  
[www.rsc.org/advances](http://www.rsc.org/advances)

### 1. Introduction

Dendrimers are attractive to researchers not only for their use in fundamental research<sup>1</sup> but also their applications in catalysis,<sup>2</sup> drug delivery, biosensors<sup>3</sup> and organic electronics<sup>4</sup> due to their unique three-dimensional dendritic structures and properties. Different functional supramolecular structures can be gained through the self-assembly of dendrons or dendrimers, which is directed by non-covalent interactions.<sup>5</sup> Through proper design and synthesis, the cores, dendrons and surface groups can all be chosen and the molecular structure of the dendrimers can be adjusted precisely. As the intermolecular interactions between the segments of dendrimers are controllable, the self-assembly process and final supramolecular structures of dendrimers can be tuned effectively.<sup>3,6</sup>

The optoelectronic properties of the  $\pi$ -conjugated materials are highly influenced by the molecular structure, and further the condensed supramolecular structure, of the molecules.<sup>7–9</sup>

Many  $\pi$ -conjugated dendrimers have been designed and found applications in organic electronics.<sup>4,10,11</sup> Several groups have studied the self-assembly behaviors of conjugated dendrimers, such as the aggregation of phenylacetylene dendrimers in solution,<sup>12,13</sup> the controlled self-assembly of polyphenylene dendrimers at the interface of solution and substrate<sup>14–16</sup> and recently the supramolecular assembly behavior of thiophene dendrimers on glass and graphite substrates.<sup>17,18</sup> The molecular structure of the conjugated dendrimers, such as the structure of the cores, dendrons and surface groups, the dendron generations and molecule shapes, the solvents and the substrates have great influence on the self-assembly process due to the different molecule–solvent–substrate interactions. Lu *et al.* found that the acetylene-linked dendrimer TP1 can self-assemble into one-dimensional nanofibers from the mixture solvent, while under the same fabrication condition no aggregates form for TP2, which contains more acetylfluorene dendrons.<sup>19</sup> Müllen *et al.* found that lower generation polyphenylene dendrimers only form nanofibers, while the higher generation dendrimers can form both nanofibers and globular clusters.<sup>14</sup> Advincula *et al.* found that the morphology of the thiophene dendrimer 14T can change from nanowires to two-dimensional crystalline structures on the graphite surface with a longer dodecyl side chain instead of a hexyl chain, which is ascribed to the increased

<sup>a</sup>State Key Laboratory of Polymer Physics and Chemistry, Changchun Institute of Applied Chemistry, Chinese Academy of Sciences, 5625 Renmin Street, Changchun 130022, P. R. China. E-mail: [ychan@ciac.jl.cn](mailto:ychan@ciac.jl.cn); Fax: 86-431-85262126;

Tel: 86-431-85262175

<sup>b</sup>University of the Chinese Academy of Sciences, 52 Sanlihe Rd., Beijing, China

† Electronic supplementary information (ESI) available. See DOI: 10.1039/c3ra23272g

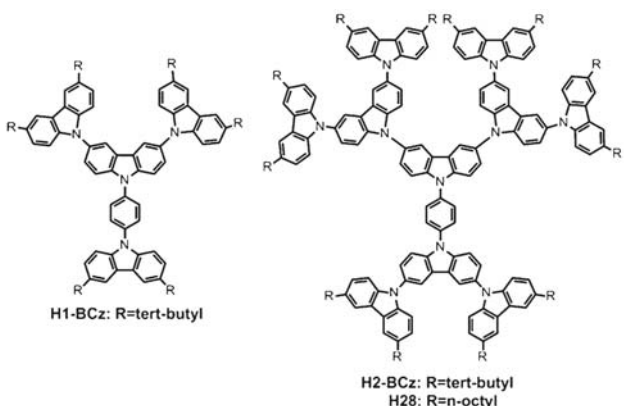
dendrimer dimensions and stronger molecule–substrate interaction.<sup>18</sup>

Carbazole compounds are widely used in organic electronics due to their excellent optical and electrical properties.<sup>20,21</sup> Carbazole dendrimers have also been designed and have found applications in organic light-emitting diodes.<sup>22–24</sup> In our previous work, we have studied the self-assembly behavior of the first generation carbazole-based conjugated dendrimer H1-BCz through SVA and found that the assemblies can vary from fibers to spherulites as the solvent vapor pressure decreases due to the different dewetting and crystallization processes.<sup>25</sup> In this work, we further studied the effects of molecular structures and the properties of the solvents on the self-assembly behavior of carbazole-based dendrimers by SVA on glass and carbon-coated glass substrates. The polar solvent THF and apolar solvent hexane were used as the annealing solvent for the SVA process. We found that the amorphous H1-BCz films change into curled fibers and dendrites in hexane vapor, unlike when they are in THF vapor. For the second generation dendrimer H2-BCz, the amorphous film did not change at low vapor pressure, and only fibers formed in THF vapor and nano-sized needle-like aggregates formed in hexane vapor at high vapor pressure conditions since the molecule–molecule interaction is dominant. For H28 with *n*-octyl as the terminal groups instead of *tert*-butyl, only dewetting took place from the thin dendrimer film for the predominant molecule–solvent interaction in both THF and hexane vapor.

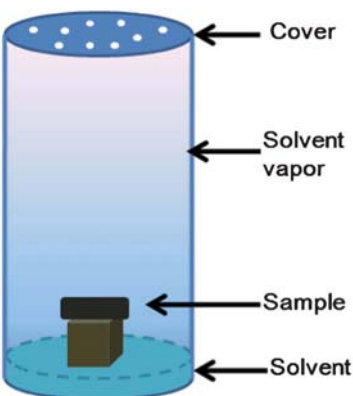
## 2. Experimental section

### 2.1. Materials

The carbazole-based dendrimers H1-BCz, H2-BCz and H28 were synthesized as previously described (ref. 26). The molecular structures of the dendrimers are shown in Scheme 1. The solvents tetrahydrofuran (THF), dichloromethane ( $\text{CH}_2\text{Cl}_2$ ), hexane and chlorobenzene were purchased from Beijing Chemical Reagent Co. Ltd., China. All the solvents were purified before used. The glass substrates were



**Scheme 1** Molecular structures of the first generation carbazole-based dendrimer H1-BCz and the second generation dendrimers H2-BCz and H28.



**Scheme 2** A schematic of the solvent-vapor annealing set.

cleaned in a piranha solution (70/30 v/v of concentrated  $\text{H}_2\text{SO}_4$  and 30%  $\text{H}_2\text{O}_2$ ) at 70 °C for 30 min, thoroughly rinsed with deionized water and dried by nitrogen blowing. The clean glass slides coated with amorphous carbon films was used as the apolar substrates.

### 2.2. Sample preparation

H1-BCz, H2-BCz and H28 were dissolved in chlorobenzene to achieve a concentration of 10 mg ml<sup>-1</sup>. All the solutions were put in a dark and vibrationless environment for 24 h at room temperature (25 °C) to obtain homogeneous samples. The solutions were filtered using 0.22 µm PTFE filters before they were used. The as-spun films were put into a vacuum oven for 24 h to remove the residual solvent. Assemblies of the dendrimers were prepared by putting the amorphous films in a nearly closed glass container (3 cm in diameter and 20 cm in length) with pre-added 10 ml THF or hexane solvent to create a saturated solvent environment as shown in Scheme 2. The different vapor pressures were obtained by tuning the distance between the sample position and the surface of the liquid solvent.<sup>27</sup> For the *in situ* observation of the self-assembly process, the container used was 4 cm in diameter and 2.5 cm in height with a transparent glass cover and had 0.05 ml THF pre-added.

### 2.3. Characterization

The surface morphology of the dendrimer films was observed using optical microscopy (Zeiss Axio Imager A2m, Carl Zeiss, Germany), atomic force microscopy (AFM) and transmission electron microscopy (TEM). AFM characterization was performed in tapping mode, using a SPA300HV with a SPI3800N controller (Seiko Instruments, Inc., Japan). A silicon microcantilever (spring constant 2 N m<sup>-1</sup> and resonance frequency ~70 kHz, Olympus Co., Japan) with an etched conical tip was used for the scan. TEM experiments were performed on a TEM-1011 (JEOL Co., Japan) with an accelerating voltage of 100 kV. TEM samples were made by exposing the films fabricated on the substrates in a HF solvent environment for 30 s and then floating these onto the water surface. Pieces of the dendrimer films were then picked up from the deionized water

surface onto a copper mesh and dried in a vacuum oven for 24 h.

Grazing incidence wide-angle X-ray diffraction (GIWAXD) was applied to determine the structural properties of the assembled thin films. All measurements were performed with the diffractometer D8 Discover (Bruker, Germany,  $\lambda = 1.54 \text{ \AA}$ ). A fixed grazing incidence angle of  $0.2^\circ$  was used to reduce the scattering from the substrates.

The UV-Vis absorption spectra were recorded using a Lambda 750 spectrometer (Perkin-Elmer, Wellesley, MA) with 5.0 nm slit. The PL and concentration-dependent luminescence spectra were recorded using a Perkin-Elmer LS 50B spectrofluorometer. The dendrimers in  $\text{CH}_2\text{Cl}_2$  with a solution concentration of  $1 \times 10^{-5} \text{ M}$  is used for the UV-Vis absorption spectra and PL spectra measurement. The amorphous films and assembled films for the spectra characterization processed in THF vapor are fabricated on quartz substrates.

### 3. Results and discussion

The effects of dendrimer generation and surface groups on the self-assembly morphology of different carbazole-based dendrimers are observed in section 3.1 and section 3.2, respectively. The effects of the molecular structures and solvent properties on the self-assembly process are discussed and the probable mechanisms are given from the viewpoint of the molecule–solvent–substrate interaction in section 3.3.

#### 3.1. The effect of generation on the self-assembly morphology of carbazole-based dendrimers

To understand the effect of generation on the self-assembly behavior of the dendrimers, we studied the film morphology evolution process of the first generation carbazole-based dendrimer H1-BCz and the second generation carbazole-based dendrimer H2-BCz.

The as-spun amorphous H1-BCz films on glass substrates change from randomly distributed fibers to spherulites due to the different dewetting processes as the THF vapor pressure decreases, which we reported previously.<sup>25</sup> Similar morphology changes were observed on apolar carbon-coated glass substrates. As shown in Fig. S1(A) to (E) (ESI†), fibers and dendrites were formed at high vapor pressure. Spherulites can be observed from the polarized optical image in Fig. S1(F') (ESI†) where the distance between the solvent liquid surface and sample position is 7.4 cm with a low vapor pressure.

While in hexane vapor on glass substrates, separated curled fibers form at a high vapor pressure with a distance of 0.6 cm between the sample position and solvent liquid surface as shown in Fig. 1 (A), dendrites barge against each other with a distance of 2.2 cm as shown in Fig. 1 (B), discrete small dendrites form with a distance of 3.8 cm as shown in Fig. 1 (C) and the morphology change is not obvious in the lower pressure conditions as shown in Fig. 1 (D). In the detailed AFM and TEM characterization, the dendrites are made up of curled fibers (Fig. 1 (F), (G), (J) and (K)). The lengths of the dendrites are about several micrometers and the widths are about tens of nanometers (Fig. 1 (E) to (G) and (I) to (K)). The film remains

amorphous at low vapor conditions with a distance of 7 cm between the sample position and solvent liquid surface as shown in Fig. 1 (H) and (L). As shown in Fig. S2 (ESI†) when apolar carbon-coated substrates were used, curled fibers also form, but the size of the dendrites is larger as shown in Fig. S2 (B) (ESI†), and the dendrites are more crowded as shown in Fig. S2 (C), ESI†. This indicates that the movability of the H1-BCz improves on a carbon-coated glass substrate compared to the movability on a glass substrate.

For the second generation dendrimer H2-BCz, only fibers are formed by SVA at high vapor pressures. From Fig. 2(A), (B) and (C) where the distance between the sample and the solvent liquid surface is 0.6 cm, 2 cm and 3.8 cm respectively, we can see that fibers have formed on the substrates. The respective polarized optical images in Fig. 2(A'), (B') and (C') show that the fibers are anisotropic, which indicates that H2-BCz molecules may crystallize in the fibers. The density of the fibers is lower and the size of the fibers is much larger in Fig. 2(A) than that in Fig. 2(B) and (C). This may be due to the higher degree of super-cooling of the swelling film under lower vapor pressures.<sup>28</sup> Though the fibers are not obvious in Fig. 2(D) and (D'), the inset AFM height image shows that there are lots of fibers formed in the films. In a much lower vapor pressure with a distance of 7.4 cm between the sample and the liquid surface (Fig. 2(E) and (E')), the film morphology does not change. The inset AFM height image in Fig. 2(E) shows that the film remains amorphous. This may be because the small amount of absorption solvent is incapable of dissolving the dendrimer molecules, the dendrimer molecules are constrained on the substrates and the self-assembly cannot take place. The morphology changes are similar on carbon-coated glass substrates.

For the second-generation carbazole-based dendrimer H2-BCz, dewetting does not take place and only fibers form during the self-assembly process at high vapor pressure. From Fig. 3(A) and (C), we can see that the morphology changes of the films are not obvious in the initial stage of SVA and dewetting does not take place at any place on the films. As time goes on, inconspicuous fibers form among the films homogeneously (Fig. 3(D)). The fibers grow thicker and longer after exposure to the THF vapor for a longer time (Fig. 3(E) and (F)). After about 1 h, the morphology does not change and the self-assembly process is complete (Fig. 3(G) and (H)). Actually, the fibers form in a much shorter time. From the inset AFM height images in Fig. 3(A) and (B), we can see that small fibers can form by exposing the as-spun amorphous films in the THF vapor for only about 2 min. As the annealing time is increased, the fibers grow thicker and longer and the fibers become curved (the inset images in Fig. 3(C), (D) and (E)). When exposing the amorphous H2-BCz films in the THF vapor for 30 min, the randomly growing fibers can cover the whole substrate (the inset image in Fig. 3(F)). Besides the large-size fibers, there are some small-size fibers distributed among the areas of large fibers in the films and a fiber network forms for the H2-BCz films. The large-size fibers and distributed small-size fibers are more obvious in the inset image in Fig. 3(G). For the large-size and small-size fiber morphology in (H) is like that in (G) both in the optical image and AFM images, thus we

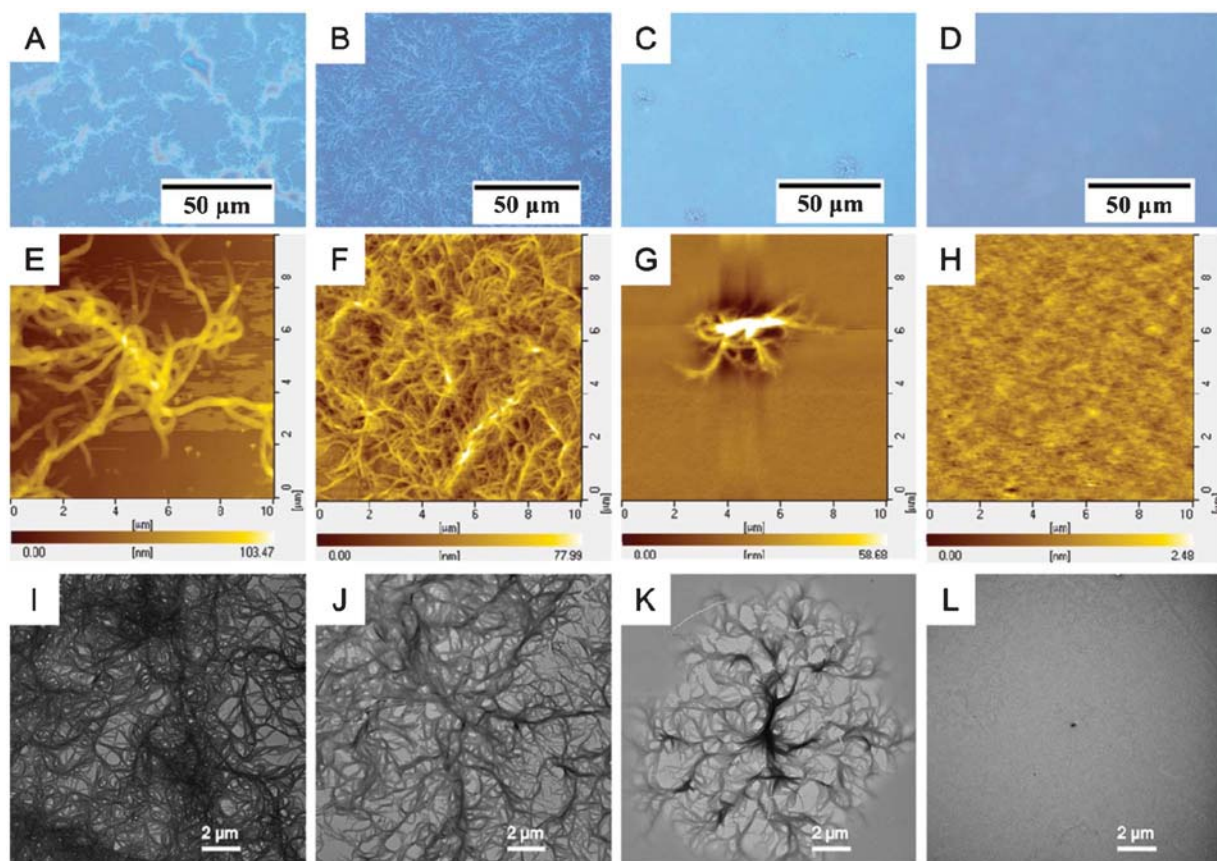


**Fig. 1** The images of the self-assembled H1-BCz fibers formed on glass substrates when exposed to different hexane vapor pressures for 16 h. (A), (B), (C), (D) are the optical images. The distances between the sample position and the solvent liquid surface are (A) 0.6 cm, (B) 2.2 cm, (C) 3.8 cm, (D) 5.4 cm. (E), (F), (G), (H) are the respective AFM height images and (I), (J), (K), (L) are the respective TEM images of (A), (B), (C), (D). The size of the AFM height images is  $10 \mu\text{m} \times 10 \mu\text{m}$ .

suppose that the self-assembly process has achieved thermodynamic equilibrium at about 1 h for H2-BCz.

While in hexane vapor, only small aggregates are formed in the H2-BCz film. As shown in Fig. 4, lots of needle-like aggregates are formed both on glass and carbon-coated glass substrates at high vapor pressure conditions. The lengths of the aggregates are about several micrometers and their widths are tens of nanometers in Fig. 4 (A) and (B). The aggregates are sparse and larger in size when the carbon-coated glass substrates are used (Fig. 4 (C) and (D)), which means that the movability of the H2-BCz molecules increases on the apolar carbon substrates.

### 3.2. The effect of surface groups on the self-assembly morphology of the carbazole-based dendrimers

To understand the effect of surface groups on self-assembly by SVA, we studied the second generation carbazole-based dendrimers H2-BCz and H28, two compounds with the same core and dendrons but different surface groups. In contrast to the fibers for H2-BCz with *tert*-butyl as the surface groups, only dewetting takes place for H28 with *n*-octyl as surface groups during the SVA process in either THF or hexane vapor both on glass and carbon-coated glass substrates.

As shown in Fig. 5, the film from H28 breaks up and dewetting takes place on the substrate under THF vapor whether under high or low vapor pressures. From Fig. 5 (F), we can see that small holes form at low vapor pressure for 30 min. As the vapor pressure increases, the size of the holes increases (Fig. 5 (B)-(E)). At higher vapor pressures, continuous films disappear and all change into small pieces of films on the substrate surface (Fig. 5 (A)). From the inset AFM height image in Fig. 5 (A), we can see that the small pieces are globular aggregates and dendrimer molecules are still in an amorphous state. By *in situ* observation of the thin film of H28 in THF vapor, we can see the whole dewetting process (Fig. S3, ESI†). The morphology of the amorphous film does not change in first three minutes, which may due to the small amount of absorbed solvent (Fig. S3 (A), ESI†). By the fourth minute, randomly distributed small holes form in the films (Fig. S3 (B), ESI†). As the time increases, the size of the holes grows larger and larger and there are some new holes formed (Fig. S3 (C), (D) and (E), ESI†). When the rims of two neighboring holes meet, discontinuous pieces of films form (Fig. S3 (E) and (F), ESI†). Unless all the continuous films break into small pieces, the dewetting process stops (Fig. S3 (G) and (H), ESI†). When carbon-coated glass is used as the substrate, similar morphological evolution is observed. When hexane is used for the

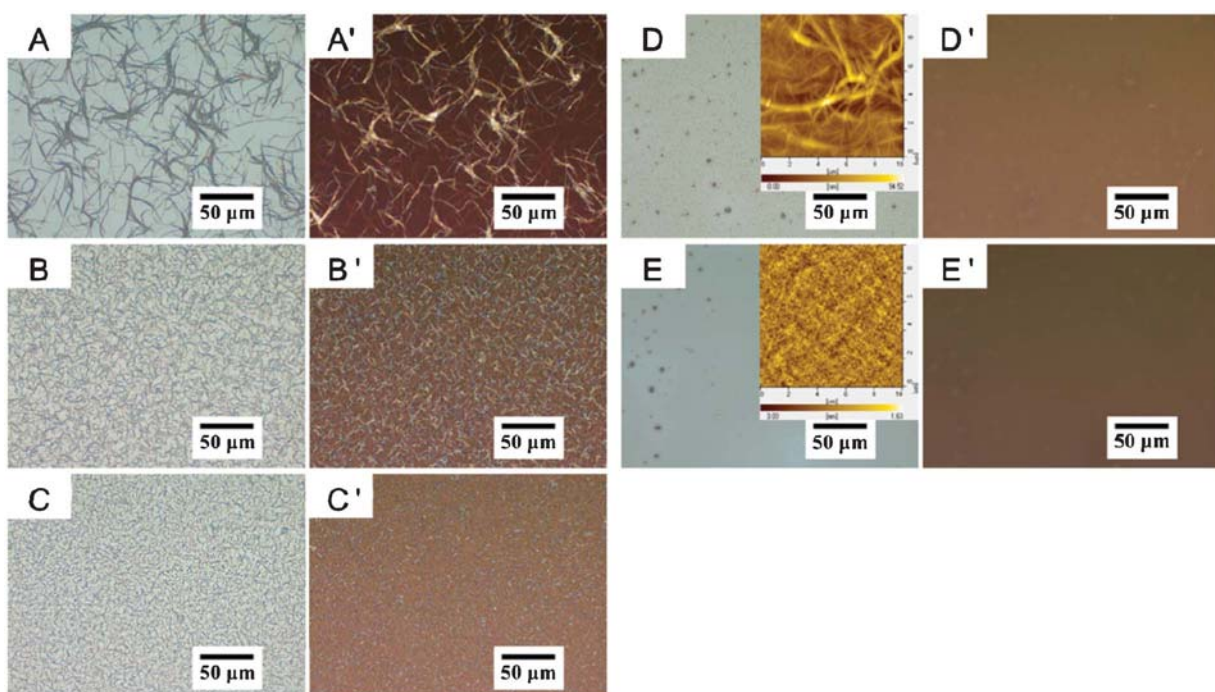


**Fig. 2** The optical images of the self-assembled H<sub>2</sub>-BCz fibers formed on glass substrates when exposed to different THF vapor pressures for 16 h. The distances between the sample position and the solvent liquid surface are (A) 0.6 cm, (B) 2.2 cm, (C) 3.8 cm, (D) 5.4 cm, (E) 7 cm. (A'), (B'), (C'), (D'), (E') are the polarized images of (A), (B), (C), (D), (E), respectively. The inset images in (D) and (E) are the AFM height images and the size of the images is 10 μm × 10 μm.

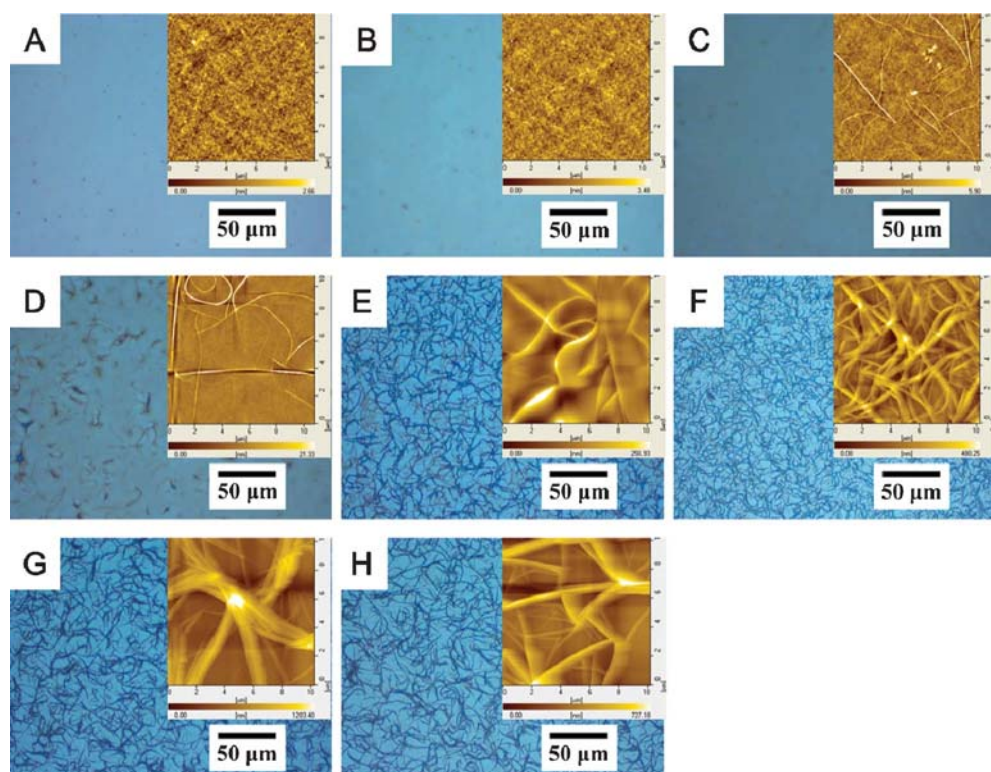


**Fig. 3** The optical images of the spin-coated H<sub>2</sub>-BCz films on glass substrates exposed to a certain THF annealing vapor pressure (the distance between the samples and the solvent liquid surface is 2cm) for different times: (A) 0 min, (B) 2 min, (C) 5 min, (D) 10 min, (E) 15 min, (F) 30 min, (G) 1 h and (H) 24 h, respectively. The inset images in (A), (B), (C), (D), (E), (F), (G) and (H) are the AFM height images and the size of these images is 10 μm × 10 μm.

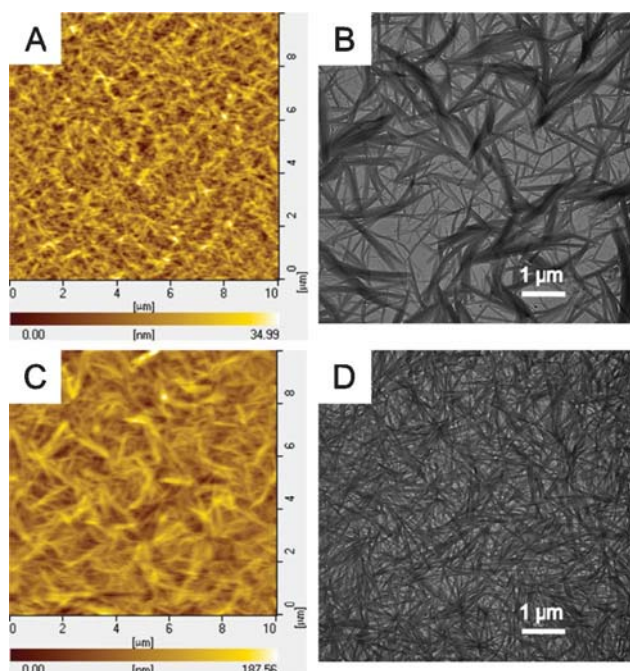


**Fig. 4** AFM height images and TEM images of the self-assembled H2-BCz fibers formed on glass and carbon-coated glass substrates when exposed to hexane vapor pressure for 16 h at a distance of 0.6 cm on different substrates: (A), (B) on glass substrates and (C), (D) on carbon-coated glass substrates. The size of AFM images is  $10 \mu\text{m} \times 10 \mu\text{m}$ .

annealing process, film breaks up and dewetting takes place, but it only happens under high vapor pressure conditions. As shown in Fig. S4, ESI,<sup>†</sup> dewetting happens when the distance between the sample position and the solvent liquid surface is 0.6 cm and 2.2 cm for H28 films in hexane vapor on both glass and carbon-coated substrates. The holes are smaller for the films on carbon-coated substrates and the dewetting processes are not so pronounced (Fig. S4 (A)–(E), ESI<sup>†</sup>). This implies that

the movability of H28 molecules decreases on carbon-coated substrates, which may be due to the better absorption of the dendrimers by the substrates caused by the apolar *n*-octyl groups.

### 3.3. The mechanism of the different self-assembly behaviors of the carbazole-based dendrimers

In the SVA process, the solvent molecules adsorb on the substrate, dissolve the deposited layer, promote the mobility of the solute molecules and promote rearrangement, which leads to the thermodynamically stable crystalline morphologies of the solutes.<sup>29–32</sup> The self-assembly process by SVA is influenced by the interactions among the solvent, solute and substrate, such as molecule–molecule, molecule–solvent, molecule–substrate and solvent–substrate interactions. Our group have demonstrated that the solvent vapor annealing processes have great influence on the self-assembly process of block copolymer film and polymer blend films.<sup>33–37</sup>

To check the effect of molecular structure on the self-assembly of the carbazole-based dendrimers, the different states of the dendrimers were studied by UV-Vis spectra and PL spectra (Fig. 6). The peaks in the absorption and PL spectra of the dilute solution and the as-spun amorphous films are similar for all the dendrimers, which indicates that dendrimer molecules in the as-spun films are dispersed as free molecules like they are in dilute solution.<sup>38</sup> The absorption and PL spectra become narrower in the amorphous films compared to in the solution, which may due to the tight packing of the molecules in the solid films and the minor intermolecular interactions in the ground state in the solid amorphous phases.<sup>39</sup> For the assembled films fabricated by SVA, there are new bands in the PL spectra. For H1-BCz films annealed in hexane vapor, the PL intensity around 370 nm increases. For crystalline films of H1-BCz from THF vapor, the new bands emerge around 370 nm and 420 nm besides the emission band around 400 nm of the individual molecules. The new bands are due to the adjacent carbazole groups forming partial or total eclipse excimers with benzene ring overlap,<sup>40</sup> which

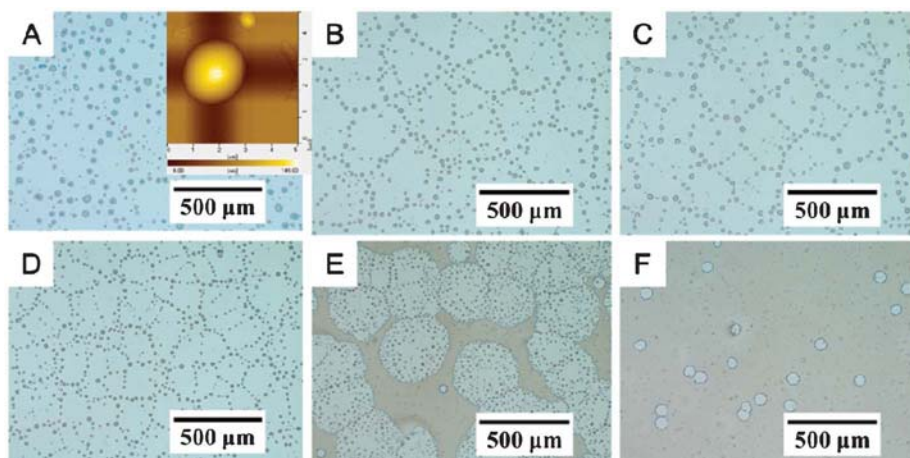


**Fig. 5** The optical images of the H28 films on a glass substrate when exposed to different THF vapor pressures for 30 min. The distances between the sample position and the solvent liquid surface are (A) 0.6 cm, (B) 2 cm, (C) 3.8 cm, (D) 5.8 cm, (E) 7.4 cm and (F) 9.4 cm, respectively. The inset in (A) is the AFM height image and the size is  $5 \mu\text{m} \times 5 \mu\text{m}$ .

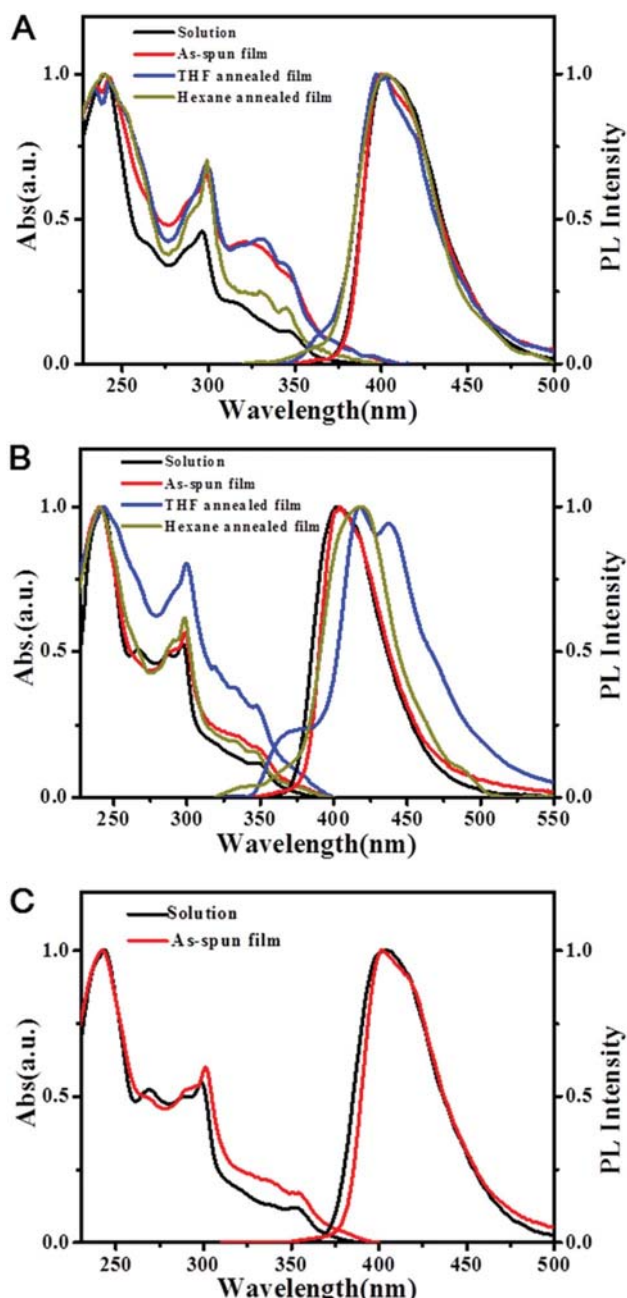


**Fig. 6** The UV-Vis absorption spectra and PL spectra of the carbazole-based dendrimers in dilute  $\text{CH}_2\text{Cl}_2$  solution (black line), amorphous films (red line), THF annealed films (blue line) and hexane annealed films (dark yellow line): (A) H1-BCz, (B) H2-BCz, (C) H28.

means that the  $\pi-\pi$  interactions are enhanced in the assembled films. The emission at 420 nm can be seen from the concentration-dependent luminescence spectra of H1-BCz at higher concentrations. As shown in Fig. S5(A), ESI,<sup>†</sup> as the solution concentration increases, the emission peak of H1-BCz red shifts from 401 nm ( $1 \times 10^{-6}$  M) to 405 ( $1 \times 10^{-4}$  M) nm and 414 nm ( $1 \times 10^{-1}$  M), respectively. The red-shift to longer wavelengths at high concentrations indicates that the ratio of excimeric emission at 420 nm is more pronounced. For

the assembled films of H2-BCz, the PL spectra changes more obviously compared to the amorphous films. For the hexane annealed H2-BCz film, the emission peak has shifted to 418 nm. For the THF annealed films, besides the red-shifted emission peak at 418 nm, new bands around 370 nm and around 450 nm emerge, which can also be ascribed to the partial and total eclipse excimers emission of the adjacent carbazole groups. From the more pronounced red-shift PL spectra of H2-BCz, we can speculate that the molecular interactions in crystalline films are much stronger for H2-BCz than for H1-BCz. The concentration-dependent luminescence spectra of H2-BCz solutions in Fig. S5(B) (ESI) demonstrate the red-shift of the H2-BCz emission at high concentration conditions. The emission peak of H2-BCz red shifts from 402 nm ( $1 \times 10^{-6}$  M) to 410 ( $1 \times 10^{-2}$  M) nm and 418 nm ( $1 \times 10^{-1}$  M), respectively, with the increase of solution concentration. We further demonstrate that the stronger molecular interactions can also enhance the gelation of H2-BCz in solvent mixtures.<sup>41</sup>

The role of the solvents in the annealing process is also vital. From the previous parts, we found that the morphology changes a lot for the carbazole dendrimers when THF is replaced by hexane. The properties of the two solvents are shown in Table 1. The boiling point and the vapor pressure are close to each other for THF and hexane. Furthermore, the contact angles for THF and hexane on glass and carbon-coated glass substrates are all about  $10^\circ$  (Table 1 and Fig. S6, ESI<sup>†</sup>). It indicates that the solvents show similar affinity for the substrates and thus the thickness of the adsorbed liquid layer on the substrates are nearly the same at the same vapor pressure conditions.<sup>42,43</sup> So the difference in morphology for the two solvents should be due to the different polarity (dielectric constant) and also the different solubility of the dendrimers. All the dendrimers dissolve well in the polar THF and the solubility is more than  $100 \text{ mg ml}^{-1}$ , while the solubility of H1-BCz and H2-BCz in the apolar hexane is small (Table 1). The increased solubility of H28 in hexane may be due to the long apolar alkyl chains attached to the polar dendrons. Compared to hexane, fibers with large size could form at relative low vapor pressure conditions for H1-BCz and H2-BCz when THF is used for the annealing process. What's more, the dendrimer molecules of H1-BCz and H2-BCz pack in a more orderly manner in the fibers formed in THF vapor. As shown in Fig. 7, the H1-BCz and H2-BCz films annealed in THF vapor show legible diffraction peaks, while no diffraction peaks are observed for the films annealed in hexane vapor. It means that H1-BCz and H2-BCz molecules move quickly and the rearrangements take place more easily in THF vapor. The influence of the solubility on the aggregation behavior of the molecules has been proved in perylenebis(dicarboximide) (PDI) derivatives.<sup>31</sup> The substrates have little influence on the self-assembling process of the dendrimers. The morphological evolutions for the dendrimers are similar on glass and carbon-coated glass substrates except for the small change in the size of the assembled structures.

The schematic of different self-assembling processes for H1-BCz, H2-BCz and H28 by SVA is shown in Fig. 8. For the first generation dendrimer H1-BCz, the number of  $\pi$ -conjugated carbazole dendrons is small and the polarity of the

**Table 1** The properties of the used solvents for solvent vapor annealing (25 °C)

Solvent	Boiling point (°C)	Vapor pressure (kPa)	Dielectric constant	Solubility (mg ml <sup>-1</sup> )			Contact angle (°)	
				H1-BCz	H2-BCz	H28	glass	carbon
THF	65.9	23.46	7.58	> 100	> 100	> 100	8	8.5
Hexane	68.7	20.00	1.89	~ 0.1	< 0.02	> 100	12.6	11.5

molecule is small. The interactions between the dendrimer molecules and the dipole–dipole interactions between molecule and substrate are weak. During self-assembling, molecule–solvent and molecule–molecule interactions are dominant. The solvent can dissolve the solute easily and dewetting takes place, while the molecules rearrange and crystallize in the areas where dewetting does not happen. For the second generation dendrimer H2-BCz, there are more polar carbazole dendrons and the polarity of the molecule is larger. The interactions between the dendrimer molecules and the dipole–dipole interactions between molecule and substrate are stronger. Thus after the solvent has dissolved the solute, the dendrimer molecules can absorb on the substrate to a certain extent and will not follow the dynamics of the solvent. Dewetting will not take place as easily as in H1-BCz films. During the self-assembly process, the molecule–molecule interactions are dominant. Thus the dendrimer molecules rearrange and crystallize into fibers. For H28, in which the surface groups are *n*-octyl instead of *tert*-butyl, the long bulk alkyl chains at the outer surface of the dendrimer distort the π–π interactions between the molecules and prevent the effective packing of the molecules. The influence of the bulk substitutes on the self-assembly process has been evidenced in PDI molecules.<sup>38,44,45</sup> Additionally, the apolar long alkyl chains decrease the dipole–dipole interactions between the dendrimer molecule and the polar substrate. The solvent molecules have better affinity to the surface of the substrate than the dendrimer molecules, which facilitates the dewetting of the

thin film.<sup>45</sup> So when H28 films were exposed to the solvent vapor, the molecule–solvent interactions are dominant. The rearrangement of the dendrimer molecules will not happen and only dewetting takes place.

#### 4. Conclusions

In conclusion, we have investigated the effects of molecular structures and the solvent properties on the self-assembly behaviors of carbazole-based dendrimers under solvent vapor annealing. The first generation dendrimer H1-BCz can change from single fibers to spherulites in THF vapor and from curled fibers to fiber dendrites in hexane vapor by decreasing vapor pressure. The second generation dendrimer H2-BCz can only form fibers in THF vapor and small needle-like aggregates in hexane vapor under high vapor pressure conditions, while for H28, which has long *n*-octyl chains as surface groups, only dewetting takes place in thin films under either THF or hexane vapor. Molecule–molecule and molecule–solvent interactions are dominant for the lower generation dendrimer H1-BCz, so dewetting takes place and molecule rearrangement and crystallization occur. Molecule–molecule interactions are dominant for H2-BCz and the molecules can rearrange and crystallize. For H28, the long chains decrease the molecule–molecule and molecule–substrate interactions and the mole-

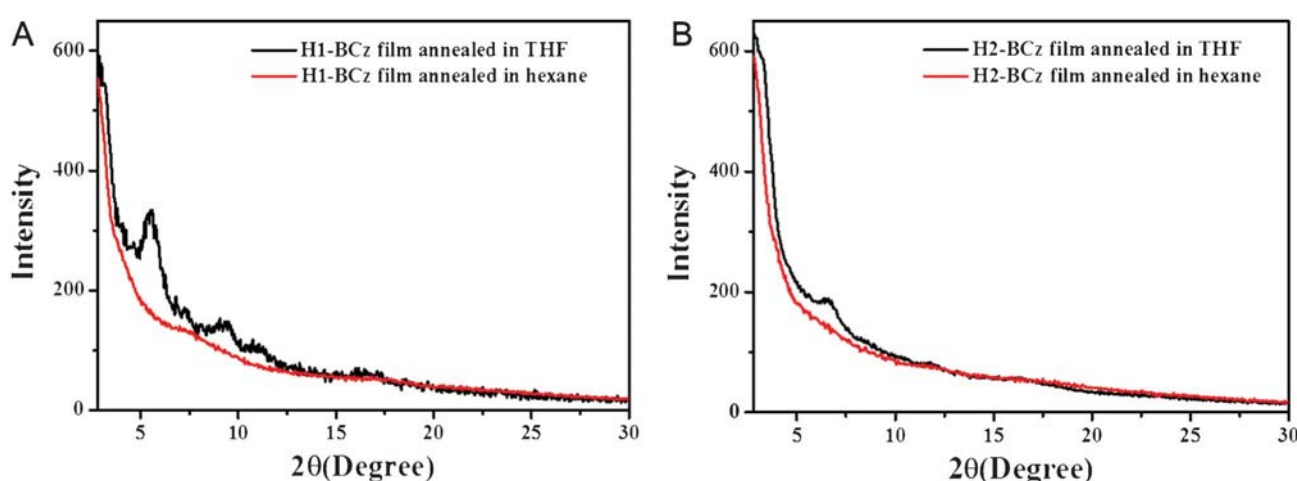


**Fig. 7** GIXD patterns of (A) H1-BCz and (B) H2-BCz film on glass substrates by exposing the as-spun film in THF (black line) and hexane (red line) vapor for 16 h. The distance between the sample and the solvent surface in (A) is 7.4 cm for THF vapor and 2.2 cm for hexane vapor, and the distance in (B) is 2.2 cm for THF vapor and 0.6 cm for hexane vapor.

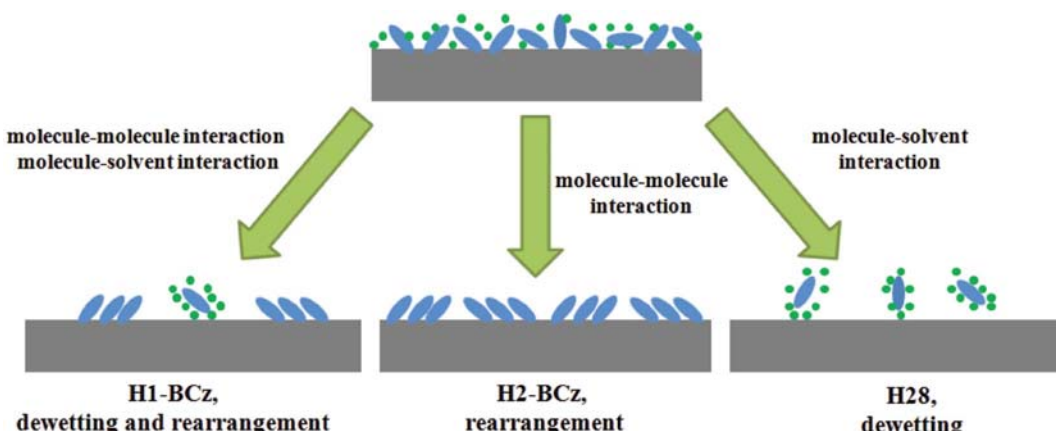


**Fig. 8** A schematic of the self-assembly behaviors for carbazole-based dendrimers by SVA.

cule–solvent interactions are dominant, so only dewetting takes place in the thin films.

## Acknowledgements

This work was financially supported by the National Natural Science Foundation of China (51273191, 51073151) and National Basic Research Program of China (973 Program-2009CB930603).

## References

- 1 A. W. Bosman, H. M. Janssen and E. W. Meijer, *Chem. Rev.*, 1999, **99**, 1665–1688.
- 2 D. Mery and D. Astruc, *Coord. Chem. Rev.*, 2006, **250**, 1965–1979.
- 3 D. Astruc, E. Boisselier and C. Ornelas, *Chem. Rev.*, 2010, **110**, 1857–1959.
- 4 S. C. Lo and P. L. Burn, *Chem. Rev.*, 2007, **107**, 1097–1116.
- 5 D. K. Smith, *Chem. Commun.*, 2006, 34–44.
- 6 B. M. Rosen, C. J. Wilson, D. A. Wilson, M. Peterca, M. R. Imam and V. Percec, *Chem. Rev.*, 2009, **109**, 6275–6540.
- 7 J. Roncali, P. Leriche and A. Cravino, *Adv. Mater.*, 2007, **19**, 2045–2060.
- 8 L. Zang, Y. K. Che and J. S. Moore, *Acc. Chem. Res.*, 2008, **41**, 1596–1608.
- 9 F. S. Kim, G. Q. Ren and S. A. Jenekhe, *Chem. Mater.*, 2011, **23**, 682–732.
- 10 P. L. Burn, S. C. Lo and I. D. W. Samuel, *Adv. Mater.*, 2007, **19**, 1675–1688.
- 11 S. H. Hwang, C. N. Moorefield and G. R. Newkome, *Chem. Soc. Rev.*, 2008, **37**, 2543–2557.
- 12 A. S. Shetty, J. S. Zhang and J. S. Moore, *J. Am. Chem. Soc.*, 1996, **118**, 1019–1027.
- 13 J. S. Moore, *Acc. Chem. Res.*, 1997, **30**, 402–413.
- 14 D. J. Liu, S. De Feyter, P. C. M. Grim, T. Vosch, D. Grebel-Koehler, U. M. Wiesler, A. J. Berresheim, K. Müllen and F. C. De Schryver, *Langmuir*, 2002, **18**, 8223–8230.
- 15 S. Loi, H. J. Butt, C. Hampel, R. Bauer, U. M. Wiesler and K. Müllen, *Langmuir*, 2002, **18**, 2398–2405.
- 16 D. J. Liu, S. De Feyter, M. Cotlet, U. M. Wiesler, T. Weil, A. Herrmann, K. Müllen and F. C. De Schryver, *Macromolecules*, 2003, **36**, 8489–8498.
- 17 C. J. Xia, X. W. Fan, J. Locklin and R. C. Advincula, *Org. Lett.*, 2002, **4**, 2067–2070.
- 18 C. J. Xia, X. W. Fan, J. Locklin, R. C. Advincula, A. Gies and W. Nonidez, *J. Am. Chem. Soc.*, 2004, **126**, 8735–8743.
- 19 Z. J. Zhao, J. H. Li, X. P. Chen, P. Lu and Y. Yang, *Org. Lett.*, 2008, **10**, 3041–3044.
- 20 J. V. Grazulevicius, P. Strohriegl, J. Pieliowski and K. Pieliowski, *Prog. Polym. Sci.*, 2003, **28**, 1297–1353.
- 21 J. F. Morin, M. Leclerc, D. Ades and A. Siove, *Macromol. Rapid Commun.*, 2005, **26**, 761–778.
- 22 J. Q. Ding, J. H. Lu, Y. X. Cheng, Z. Y. Xie, L. X. Wang, X. B. Jing and F. S. Wang, *Adv. Funct. Mater.*, 2008, **18**, 2754–2762.
- 23 F. Loiseau, S. Campagna, A. Hameurlaine and W. Dehaen, *J. Am. Chem. Soc.*, 2005, **127**, 11352–11363.
- 24 K. Albrecht and K. Yamamoto, *J. Am. Chem. Soc.*, 2009, **131**, 2244–2251.
- 25 Z. C. Ding, R. B. Xing, L. D. Zheng, Y. Sun, X. D. Wang, J. Q. Ding, L. X. Wang and Y. C. Han, *J. Phys. Chem. B*, 2011, **115**, 15159–15166.
- 26 J. Q. Ding, B. H. Zhang, J. H. Lu, Z. Y. Xie, L. X. Wang, X. B. Jing and F. S. Wang, *Adv. Mater.*, 2009, **21**, 4983–4986.
- 27 G. H. Lu, L. G. Li and X. N. Yang, *Small*, 2008, **4**, 601–606.
- 28 E. J. W. Crossland, K. Rahimi, G. Reiter, U. Steiner and S. Ludwigs, *Adv. Funct. Mater.*, 2011, **21**, 518–524.
- 29 D. J. Mascaro, M. E. Thompson, H. I. Smith and V. Bulovic, *Org. Electron.*, 2005, **6**, 211–220.
- 30 G. De Luca, A. Liscio, P. Maccagnani, F. Nolde, V. Palermo, K. Müllen and P. Samori, *Adv. Funct. Mater.*, 2007, **17**, 3791–3798.
- 31 G. De Luca, A. Liscio, F. Nolde, L. M. Scolaro, V. Palermo, K. Müllen and P. Samori, *Soft Matter*, 2008, **4**, 2064–2070.
- 32 K. C. Dickey, J. E. Anthony and Y. L. Loo, *Adv. Mater.*, 2006, **18**, 1721–1726.
- 33 W. H. Huang, C. X. Luo, B. Y. Li and Y. C. Han, *Macromolecules*, 2006, **39**, 8075–8082.
- 34 Y. H. Wei, B. Y. Li, Y. C. Han and C. Y. Pan, *Soft Matter*, 2008, **4**, 2507–2512.
- 35 P. Yang and Y. C. Han, *Langmuir*, 2009, **25**, 9960–9968.

- 36 C. X. Luo, W. H. Huang and Y. C. Han, *Macromol. Rapid Commun.*, 2009, **30**, 515–520.
- 37 J. G. Liu, Y. Sun, X. A. Gao, R. B. Xing, L. D. Zheng, S. P. Wu, Y. H. Geng and Y. C. Han, *Langmuir*, 2011, **27**, 4212–4219.
- 38 K. Balakrishnan, A. Datar, T. Naddo, J. L. Huang, R. Oitker, M. Yen, J. C. Zhao and L. Zang, *J. Am. Chem. Soc.*, 2006, **128**, 7390–7398.
- 39 Y. H. Kim, H. C. Jeong, S. H. Kim, K. Y. Yang and S. K. Kwon, *Adv. Funct. Mater.*, 2005, **15**, 1799–1805.
- 40 P. S. Chung and P. H. Holloway, *J. Appl. Polym. Sci.*, 2009, **114**, 1–9.
- 41 Z. C. Ding, Q. Q. Zhao, R. B. Xing, X. D. Wang, J. Q. Ding, L. X. Wang and Y. C. Han, *J. Mater. Chem. C*, 2013, **1**, 786–792.
- 42 E. Treossi, A. Liscio, X. L. Feng, V. Palermo, K. Müllen and P. Samori, *Small*, 2009, **5**, 112–119.
- 43 R. C. Savage, E. Orgiu, J. M. Mativetsky, W. Pisula, T. Schnitzler, C. L. Eversloh, C. Li, K. Mullen and P. Samori, *Nanoscale*, 2012, **4**, 2387–2393.
- 44 K. Balakrishnan, A. Datar, R. Oitker, H. Chen, J. M. Zuo and L. Zang, *J. Am. Chem. Soc.*, 2005, **127**, 10496–10497.
- 45 A. Datar, R. Oitker and L. Zang, *Chem. Commun.*, 2006, 1649–1651.